J Solid State Electrochem (2010) 14:851–855
DOI 10.1007/s10008-009-0865-7

ORIGINAL PAPER

Electrochemical discharge performance of Mg-Li based alloys in NaCl solution

Dianxue Cao · Xue Cao · Guiling Wang · Lin Wu · Zhanshuang Li

Received: 30 March 2009 / Revised: 4 May 2009 / Accepted: 11 May 2009 / Published online: 2 June 2009

Abstract Mg–Li–Al–Sn and Mg–Li–Al–Sn–Ce alloys were prepared using a vacuum induction melting method. Their electrochemical oxidation behavior in NaCl solution was investigated by means of potentiodynamic and chronoamperometric measurements. The surface morphology after discharge was examined using scanning electron microscopy. Utilization efficiency was estimated with a mass-loss method. The results indicated that Mg–Li–Al–Sn has a higher discharge current density but lower utilization efficiency than Mg–Li–Al–Sn–Ce. The typical utilization efficiency after continuous discharging at constant potential of −1.0 for 2 h is 65% and 70% for Mg–Li–Al–Sn and Mg–Li–Al–Sn–Ce, respectively. The utilization efficiency decreased with the increase of anodic potential. Both alloys have similar self-discharge rate in NaCl solution at open-circuit potential.

Keywords Mg–Li–Al–Sn · Mg–Li–Al–Sn–Ce · Discharge behavior · Metal semi-fuel cell · Anode material

Introduction

$Mg–H_2O_2$ semi-fuel cells have been studied as undersea power sources due to their high energy density, stable discharging ability, short mechanical recharge time, long dry storage life, ability to work at ambient pressure, environmental acceptability, reliability, safety, and low cost [1–8]. Magnesium as anode has the advantages of high Faradic capacity, high specific energy, more negative standard electroreduction potentials, and high discharge performance in seawater electrolyte [9]. Medeiros et al. [1] investigated $Mg–H_2O_2$ semi-fuel cells, using magnesium alloy AZ61 as anode, carbon fiber supported Pd–Ir as cathode catalyst, $H_2O_2 + H_2SO_4$ as cathode-active components, seawater as electrolyte, and Nafion-115 as membrane. The cell has a theoretical voltage of 4.14 V. The practical cell voltage is above 1.7 V at 25 mA cm^{-2} with magnesium and hydrogen peroxide efficiencies ranging from 77% to 86% and specific energies ranging from 500 to 520 Wh kg^{-1} based on the weights consumed during discharge of the magnesium anode, hydrogen peroxide, and acid.

Thermodynamically, magnesium anodes should exhibit very negative potentials. However, in practice, these electrodes operate at significantly less negative potentials because (a) magnesium is normally covered by passive oxide films which cause a delay in reaching a steady state and reduce discharging rate; (b) magnesium undergoes parasitic corrosion reactions or self discharge, resulting in the reduction of Columbic efficiency (less than 100% utilization of the metal) and the evolution of hydrogen. There are, in general, two ways to improve the anode performance. One is to dope the magnesium with other elements. The second is to modify the electrolyte by including additives. Both methods can prohibit the formation and/or accelerate the elimination of oxide layers as well as suppress corrosive dissolution.

The improvement of magnesium anode performance by the addition of alloying elements to pure magnesium has not been well investigated. Udhayan et al. [10] reported that magnesium alloy AP65 (Al, 6–7%; Pb, 4.5–5%; Zn, 0.14–1.5%; Mn, 0.15–1.3%) has a hydrogen evolution rate of 0.15 cm^{-3} min^{-1} cm^{-2} and a utilization efficiency of 84.6%. The open-circuit potential of this alloy is −1.803 V (vs.

D. Cao (✉) · X. Cao · G. Wang · L. Wu · Z. Li
Key Laboratory of Superlight Materials & Surface Technology, Ministry of Education, Harbin Engineering University, Harbin 150001, People's Republic of China
e-mail: caodianxue@hrbeu.edu.cn

saturated calomel reference electrode (SCE)) measured in seawater. Sivashanmugam et al. [11] found that Mg–Li alloy, with 13 wt.% Li for possible use in magnesium primary reserve batteries, exhibited higher anodic efficiency and offered higher operating voltage and capacity than the conventionally used Mg–Al alloy in the Mg–Li/$MgCl_2$/CuO cell. Recently, we studied the discharge performance of Mg–Li based alloys, such as Mg–Li, Mg–Li–Al, Mg–Li–Al–Ce, Mg–Li–Al–Ce–Zn, and Mg–Li–Al–Ce-Zn–Mn, in NaCl solution and found that these alloys exhibited superior electrooxidation activity and utilization efficiency [6, 12].

In this study, Mg–Li–Al–Sn and Mg–Li–Al–Sn–Ce alloys were prepared. Their discharge performance in NaCl solution (the electrolyte for Mg–H_2O_2 semi-fuel cell and magnesium seawater battery) was studied. The discharge activity and utilization efficiency of these magnesium alloy anodes at various potentials were investigated.

Experimental

Preparation of magnesium alloys

Mg–Li–Al–Sn and Mg–Li–Al–Sn–Ce alloys were prepared from ingots of pure element of magnesium (99.99%), lithium (99.99%), aluminum (99.99%), tin (99.99%), and Mg–Ce alloy containing 26.6 wt.% Ce using a vacuum induction melting furnace. Details of the procedure can be found in [6, 12]. In brief, ingots of the pure element and the alloy were charged into an induction furnace and melted under the protection of ultrahigh purity argon. The molten alloys were then poured through a tundish into a stainless steel cylindrical can mold with an inner diameter of 6 cm and a height of 18 cm and cooled down to ambient temperature under an argon atmosphere. The resulting alloys, of composition given in Table 1, were used in their cast state.

The alloy ingots were machined to 20×20×2 mm to serve as the working electrode for electrochemical measurements. Prior to each experiment, the alloy surface facing the electrolyte was mechanically polished with 700 and 1,200 grit SiC abrasive papers, degreased with acetone, washed with deoxygenated ultrapure water (Milli-Q), and immediately assembled in the electrochemical cell.

Table 1 Nominal composition of the alloys (wt.%)

Alloys	Mg	Li	Al	Sn	Ce
Mg–Li–Al–Sn	87.1	8.5	3.2	1.2	–
Mg–Li–Al–Sn–Ce	85.9	8.5	3.2	1.2	1.2

Electrochemical measurements

Electrochemical measurements were carried out in a homemade three-electrode electrochemical cell with a blackened platinum gauze auxiliary electrode and a saturated calomel reference electrode [6, 12]. The metal alloy working electrodes have an exposure area of 0.95 cm^2, which was used to calculate the current density. All measurements were carried out at room temperature in 0.7 mol dm^{-3} NaCl solution which was purged with argon before transferred to the cell. All solutions were made with analytical-grade chemical reagents and Milli-Q water (Millipore, resistivity>18 MΩ cm). The potentiodynamic and chronoamperometric curves were recorded using a computerized VMP3/Z potentiostat (Princeton Applied Research) controlled by EC-lab software. All potentials were referred to the SCE reference electrode.

The utilization efficiencies were measured as follows: The weighted alloy coupons were discharged at constant potential, and current–time curves were recorded. The discharged alloy coupons were weighed after the removal of discharge products. The alloy utilization efficiency (η) was calculated using Eq. 1 [6].

$$\eta = \frac{(Q/nF)M_a}{W_i - W_f} \times 100\% \quad (1)$$

$$n = \sum x_i z_i \quad (2)$$

$$M_a = \sum x_i M_i \quad (3)$$

where Q is the charge in Coulombs obtained by the integration of current–time curve; F is Faraday constant (96,485 C mol^{-1}); W_i and W_f are the weights of alloy sample in grams before and after discharge, respectively; n is the average number of electrons per discharge reaction assuming the oxidation states of the products are 2+ for Mg, 1+ for Li, and 3+ for Al, Sn, and Ce. M_a is the average atomic mass (g mol^{-1}) of the sample. n and M were calculated by Eqs. 2 and 3, respectively, where x_i is the mole fraction, z_i is the oxidation state, and M_i is the atomic mass of component i.

Results and discussion

Potentiodynamic polarization

Figure 1 shows potentiodynamic polarization curves of Mg–Li–Al–Sn and Mg–Li–Al–Sn–Ce measured in 0.7 mol dm^{-3} NaCl solution at a scan rate of 5 mV s^{-1} taken after

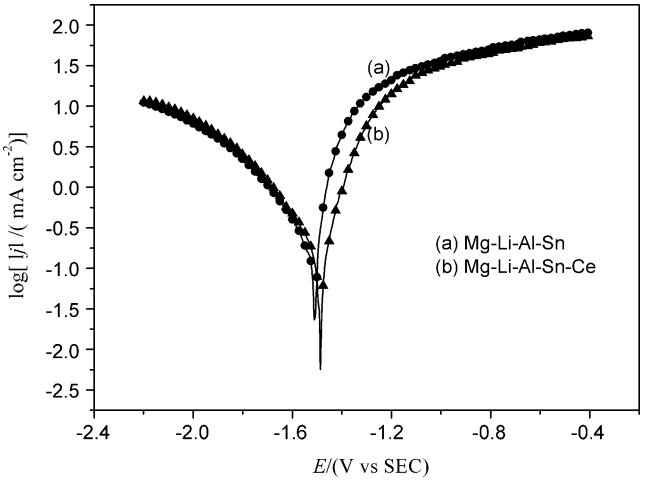

Fig. 1 Potentiodynamic polarization curves for Mg–Li–Al–Sn and Mg–Li–Al–Sn–Ce measured in 0.7 mol dm^{-3} NaCl solution at a scan rate of 5 mV s^{-1}

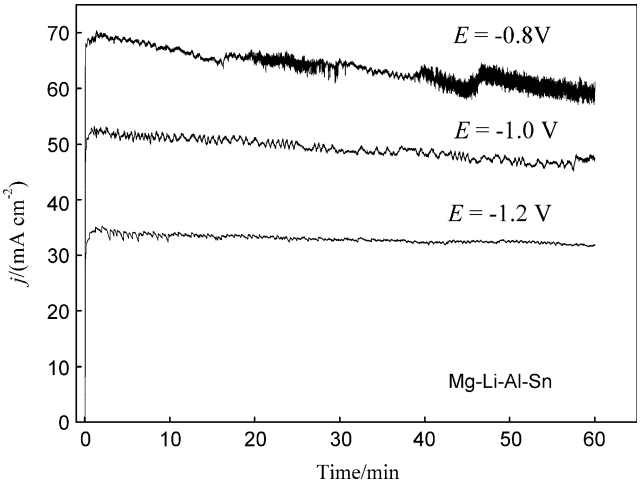

Fig. 2 Current–time curves for Mg–Li–Al–Sn recorded in 0.7 mol dm^{-3} NaCl solution at various anodic potentials

the alloys are discharged at −1.4 V for 20 min. The corrosion potential of Mg–Li–Al–Sn is slightly more cathodic than that of Mg–Li–Al–Sn–Ce (~25 mV). The anodic current densities of Mg–Li–Al–Sn are larger than those of Mg–Li–Al–Sn–Ce, particularly in the potential range of −1.5 to −1.0 V. At higher anodic potentials, the current plateau values are similar for both alloys. These results indicate that the two alloys have a different discharge behavior. The difference can be associated with different chemical compositions of the magnesium alloy samples. Although the standard potential of the magnesium electrode is −2.612 V vs. SCE, the onset oxidation potential is observed to be about −1.50 V vs. SCE. The deviation in potential is due to the formation of oxidation products on the alloy surface.

Chronoamperometric measurements

Chronoamperometric measurements at various anodic potentials are carried out to evaluate the discharge performance of Mg–Li–Al–Sn and Mg–Li–Al–Sn–Ce. Figures 2 and 3 show that the current–time profiles are similar for both samples, i.e., the anodic currents increase rapidly in the early discharging stage, reach a maximum value about 1.5 min, and then decrease slightly. For both samples, the currents decrease relatively faster at higher anodic potentials (larger discharge currents), which can be attributed to the fast rate of formation and accumulation of oxidation products on the alloy surfaces at high discharge currents. The larger vibration in discharge currents at a higher anodic potential, such as −0.8 V, is an indication of the surface film formation. Comparison of Figs. 2 and 3 demonstrates that Mg–Li–Al–Sn exhibits higher discharge current densities than that of Mg–Li–Al–Sn–Ce at all anodic potentials measured. The anodic current density after 1 h discharge at −0.8 V is about 60 mA cm^{-2} for Mg–Li–Al–Sn and about 45 mA cm^{-2} for Mg–Li–Al–Sn–Ce alloy. Clearly, Mg–Li–Al–Sn is better than Mg–Li–Al–Sn–Ce in terms of discharge activity.

The surface morphology of Mg–Li–Al–Sn after discharge at low and high anodic potentials is investigated by scanning electron microscopy. Figure 4a, b shows the scanning electron microscope (SEM) image of Mg–Li–Al–Sn after discharge for 60 min at −1.2 V and −0.8 V, respectively. It can be seen that, after discharge at −1.2 V for 60 min (Fig. 4a), most parts of the alloy surface are covered by relatively small and loosely packed aggregates, while some portions of the initial surface area remain uncovered. However, after discharge at −0.8 V for 60 min (Fig. 4b), the alloy surface is completely covered by relatively large and dense aggregates. The difference in

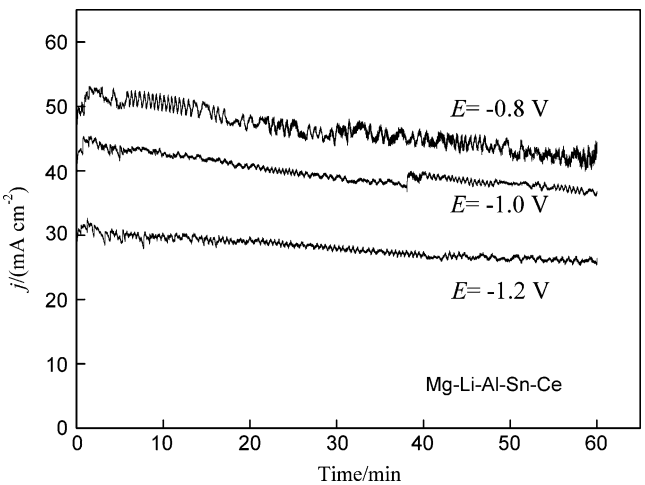

Fig. 3 Current–time curves for Mg–Li–Al–Sn–Ce recorded in 0.7 mol dm^{-3} NaCl solution at various anodic potentials

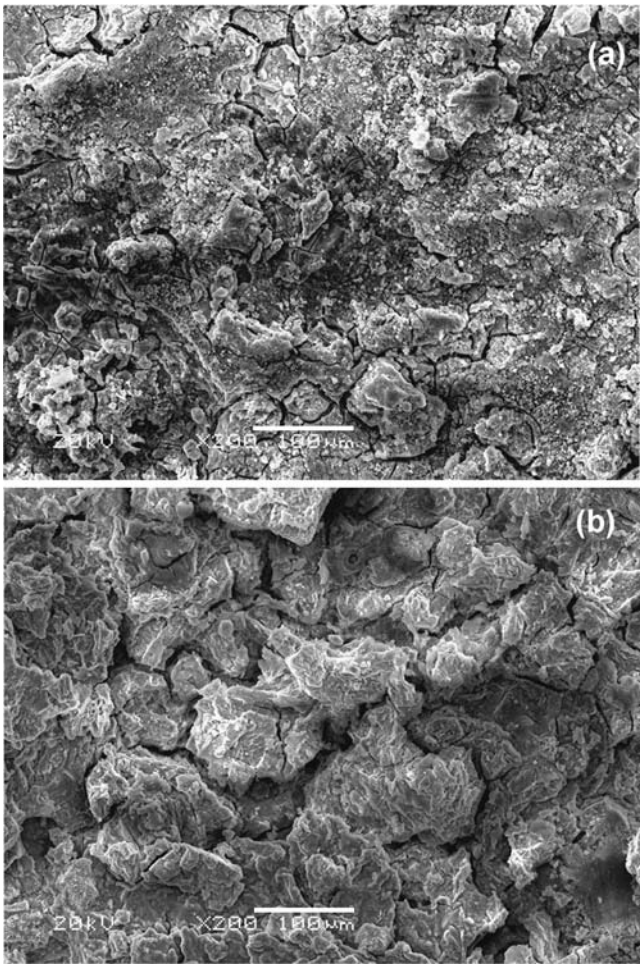

Fig. 4 SEM images of Mg–Li–Al–Sn after discharge for 60 min at −1.2 V (**a**) and −0.8 V (**b**)

the surface layer formed at low and high discharge potentials explains the different discharge behavior shown in Fig. 2. The electrode surface was less passivated when discharged at lower anodic potentials. The effective area of electrode/electrolyte interface for discharge reaction to occur is relatively more steady at low anodic potential than at higher anodic potential. Consequently, the discharge currents at lower anodic potentials are more stable and less noisy (Fig. 2).

The dependence of utilization efficiencies of Mg–Li–Al–Sn and Mg–Li–Al–Sn–Ce alloys on discharge potentials is investigated. Table 2 gives the utilization efficiencies of Mg–Li–Al–Sn and Mg–Li–Al–Sn–Ce discharged at different potentials each for 1 h. It can be seen that the utilization efficiency decreases with the increase of discharge potential for both samples. The utilization efficiency of Mg–Li–Al–Sn is nearly the same as Mg–Li–Al–Sn–Ce at −1.4 V. But at potentials more positive than −1.4 V, Mg–Li–Al–Sn–Ce shows higher utilization efficiency. The low utilization efficiency at high discharge potential might be partly due to

Table 2 Utilization efficiencies of Mg–Li–Al–Sn and Mg–Li–Al–Sn–Ce alloys discharged at various potentials for 1 h

Alloys	Utilization efficiency η (%)			
	−1.4V	−1.2V	−1.0V	−0.8V
Mg–Li–Al–Sn	81±2	72±1.5	68±1	63±1
Mg–Li–Al–Sn–Ce	80±2	76±1.5	73±1	68±1

the incomplete oxidation of alloys at fast discharge rates, that is, some of the metals might be enwrapped and isolated during discharge by the insulating oxidation products. The utilization efficiency reduces from about 81% to 63% for Mg–Li–Al–Sn and from about 80% to 68% for Mg–Li–Al–Sn–Ce as the discharge potential increases from −1.4 to −0.8 V. These results demonstrate that Ce addition suppresses self-discharge of the alloy to some extent during discharge.

Utilization efficiency losses caused by self-discharge at open circuit potential are measured by continuous and intermittent discharge experiments. First, the alloys were continuously discharged at −1.0 V for 2 h. Then fresh alloy samples were discharged at −1.0 V for 1 h, left at open circuit potential for 24 h in the electrolyte, and discharged at −1.0 V for another hour. The typical current–time curves for the continuous (test #1) and intermittent(test #2) discharge of Mg–Li–Al–Sn–Ce are shown in Fig. 5. The utilization efficiency is 65% for Mg–Li–Al–Sn and 70% for Mg–Li–Al–Sn–Ce after continuous discharge and is 61% for Mg–Li–Al–Sn and 68% for Mg–Li–Al–Sn–Ce after intermittent discharge. So the utilization efficiency loss resulting from self-discharge in the electrolyte at open circuit potential in 24-h period is 4% and 2% for Mg–Li–Al–Sn and Mg–Li–

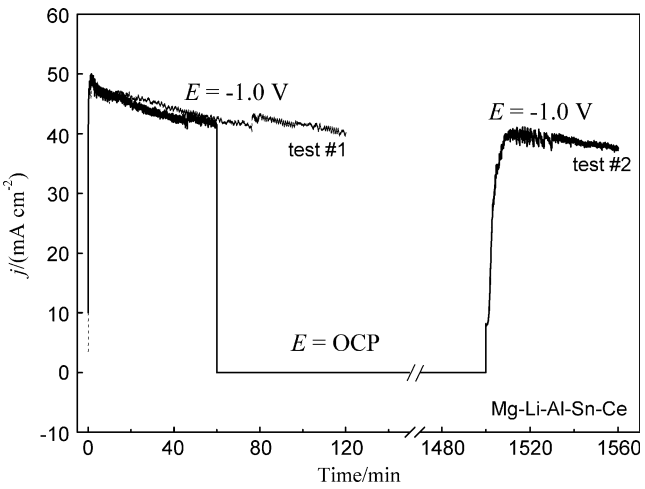

Fig. 5 Typical current–time curves for Mg–Li–Al–Sn–Ce recorded in 0.7 mol dm^{-3} NaCl solution. *Test #1* continuous discharge at −1.0 V for 2 h. *Test #2* discharge at −1.0 V for 1 h, open circuit potential for 24 h, and −1.0 V for another hour

Al–Sn–Ce, respectively. These measurements demonstrated that the two alloys show no obvious difference in the rate of self-discharge at open circuit potential.

Conclusions

Casting ingots of Mg–Li–Al–Sn and Mg–Li–Al–Sn–Ce alloys are prepared by the induction melting method. Their discharge behavior in NaCl solution is investigated. Mg–Li–Al–Sn displays higher discharge current density than Mg–Li–Al–Sn–Ce under the same discharge potential between −1.4 V and −0.8 V. However, Mg–Li–Al–Sn–Ce has higher utilization efficiency than Mg–Li–Al–Sn. Utilization efficiency depends upon discharge potential, and it decreases with the increase of anodic potential. The utilization efficiency after continuous discharging at constant potential of −1.0 for 2 h is 65% and 70% for Mg–Li–Al–Sn and Mg–Li–Al–Sn–Ce, respectively. These results indicate that Mg–Li–Al–Sn has higher discharge activity but lower utilization efficiency than Mg–Li–Al–Sn–Ce.

Acknowledgments We gratefully acknowledge the financial support of this research by Heilongjiang Provincial Natural Science Foundation (ZJG2007-06-02), Heilongjiang Postdoc Foundation (LBH-Q06091), and Harbin Engineering University (HEUFT07030).

References

1. Medeiros MG, Bessette RR, Deschenes CM, Patrissi CJ, Carreiro LG, Tucker SP, Atwater DW (2004) J Power Sources 136:226–231. doi:10.1016/j.jpowsour.2004.03.024
2. Medeiros MG, Bessette RR, Deschenes CM, Atwater DW (2001) J Power Sources 96:236–239. doi:10.1016/S0378-7753(01)00500-6
3. Medeiros MG, Dow EG (1999) J Power Sources 80:78–82. doi:10.1016/S0378-7753(98)00253-5
4. Bessette RR, Medeiros MG, Patrissi CJ, Deschenes CM, LaFratta CN (2001) J Power Sources 96:240–244. doi:10.1016/S0378-7753(01)00492-X
5. Yang W, Yang S, Sun W, Sun G, Xin Q (2006) Electrochim Acta 52:9–14. doi:10.1016/j.electacta.2006.03.066
6. Cao D, Wu L, Wang G, Lv Y (2008) J Power Sources 183:799–804. doi:10.1016/j.jpowsour.2008.06.005
7. Hasvold O, Storkersen NJ, Forseth S, Lian T (2006) J Power Sources 162:935–942. doi:10.1016/j.jpowsour.2005.07.021
8. Hasvold O, Lian T, Haakaas E, Storkersen N, Perelman O, Cordier S (2004) J Power Sources 136:232–239. doi:10.1016/j.jpowsour.2004.03.023
9. Hamlen RP, Atwater DW in: D. Linden, and T.B. Reddy, (Eds.), Handbook of Batteries, McGraw-Hill. 381.
10. Udhayan R, Muniyandi N, Mathur PB (1992) Br Corros J 27:68–71
11. Sivashanmugam A, kumar TP, Renganathan NG, Gopukumar S (2004) J Appl Electrochem 34:1135–1139. doi:10.1007/s10800-004-2728-3
12. Cao D, Wu L, Sun Y, Wang G, Lv Y (2008) J Power Sources 177:624–630. doi:10.1016/j.jpowsour.2007.11.037